Vibrational Circular Dichroism and IR Spectral Analysis as a Test of Theoretical Conformational Modeling for a Cyclic Hexapeptide

PETR BOUR,[1,2] JOOHYUN KIM,[1] JOSEF KAPITAN,[1,2] ROBERT P. HAMMER,[3] RONG HUANG,[1] LING WU,[1] AND TIMOTHY A. KEIDERLING[1]*

[1]*Department of Chemistry, University of Illinois at Chicago, Chicago, Illinois*
[2]*Institute of Organic Chemistry and Biochemistry, Academy of Sciences, Prague 6, Czech Republic*
[3]*Department of Chemistry, Louisiana State University, Baton Rouge, Louisiana*

ABSTRACT A model cyclohexapeptide, cyclo-(Phe-^{D}Pro-Gly-Arg-Gly-Asp) was synthesized and its IR and VCD spectra were used as a test of density functional theory (DFT) level predictions of spectral intensities for a peptide with a nonrepeating but partially constricted conformation. Peptide structure and flexibility was estimated by molecular dynamics (MD) simulations and the spectra were simulated using full quantum mechanical (QM) approaches for the complete peptide and for simplified models with truncated side chains. After simulated annealing, the backbone conformation of the ring structure is relatively stable, consisting of a normal β-turn and a tight loop (no H-bond) which does not vary over short trajectories. Only in quite long MD runs at high temperatures do other conformations appear. MD simulations were carried out for the cyclic peptide in water and in TFE, which match experimental solvents, as well as with and without protonation of the Asp carboxyl group. DFT spectral simulations were made using the annealed structure and were extended to include basis set variation, to determine an optimal computational approach, and solvent simulation with a polarized continuum model (PCM). Stepwise full DFT simulation of spectra was done for various sequences with the same backbone geometry but based on (1) solely Gly residues, (2) Ala substitution except Gly and Pro, and (3) complete sequences with side chains. Additionally, a selection of structures was used to compute IR and VCD spectra with the optimal method to determine structural variation effects. The side chains, especially the Asp—COOH and Arg—NH_2 transitions, had an impact on the computed amide frequencies, IR intensities and VCD pattern. Since experimentally these groups would have little chirality, due to conformational variation, they do not impact the observed VCD spectra. Correcting for frequency shifts, the Ala model for the cyclopeptide gives the clearest representation of the amide VCD. The experimental sign pattern for the amide I' band in D_2O and also the sharper, more intense amide I VCD band in TFE was seen to some degree in one conformer with Type II′ turns, but the data favor a mix of structures. *Chirality 20:1104–1119, 2008.*

KEY WORDS: peptide conformational spectral interpretation; infrared absorption; vibrational circular dichroism; density functional theory; molecular dynamics; solvent effects

INTRODUCTION

Vibrational spectroscopy has a long history in the conformational analyses of peptide structures.[1] Originally empirical correlations of IR amide I and II frequency positions were first used to discriminate helical and sheet-like peptides, then extended to protein studies, after which Raman analyses of amide I and III frequencies were applied to proteins. More recently the chiroptical variants of both were utilized to distinguish protein conformations and to deconvolve components of mixed structures as found in globular proteins.[2–6] Of the structural types, α-helices and β-sheets yield the more characteristic vibrational transitions, since they are repeating structures of some

Contract grant sponsor: National Science Foundation; Contract grant numbers: CHE-0316014, CHE-0718543 to TAK
Contract grant sponsor: American Chemical Society; Contract grant numbers: 42027-AC4 to RPH
Contract grant sponsor: Grant Agency of the Czech Republic; Contract grant numbers: 203/06/0420, 202/07/0732 to PB
Contract grant sponsor: Grant Agency of the Academy of Sciences; Contract grant number: A400550702 to PB
Contract grant sponsor: John Simon Guggenheim Fellowship to TAK
*Correspondence to: Timothy A. Keiderling, Department of Chemistry, University of Illinois at Chicago, Chicago, Illinois. E-mail: tak@uic.edu
Received for publication 2 September 2007; Accepted 7 February 2008
DOI: 10.1002/chir.20560
Published online 27 May 2008 in Wiley InterScience (www.interscience.wiley.com).

uniformity in amide conformation, resulting in excitonic bands of higher intensity and characteristic chirality. This has led to a number of useful analyses and, for peptides, to some exceptionally detailed spectral assignments, recently enhanced by use of isotopic labeling to create localized transitions.[7–18] A key element of peptide conformational studies is use of chiroptical techniques such as circular dichroism (CD) and more recently vibrational CD (VCD) and Raman optical activity (ROA), the latter of which can have useful sensitivity to isotopic variants.[4–6,14,19–21] Here chirality is not used to determine absolute configuration, which is, of course, known from the synthetic method used (e.g. employing L-amino acids), but is useful to determine oligomer conformation which can be uniform (as in helices or sheets) or highly variable, lacking repeating character, particularly in ϕ, ψ torsions. Conformational chirality is most strongly evident for the amide properties which would otherwise be locally achiral without interresidue coupling in the oligomer.

A major conformational contribution to globular protein structure comes from the various turn structures by which a strand can reverse itself in space and make the protein or peptide more compact. By its very nature these are not repetitive and thus do not give a uniform contribution to the spectrum nor create extended exciton coupled modes. Spectral characterization of turns has been a long term goal in conformational analyses, with most attention on tight β-turns that reverse the strand direction and form a H-bond from position i (C=O) to $i + 3$ (N—H).[22–27] Creating viable experimental models of stable turn peptides is challenging as well. If a turn is part of a linear peptide chain there will be considerable local conformational fluctuation unless some other construct constrains it, thereby creating a large energy barrier to transformation. One method to constrain a turn is formation of a hairpin, a topic that has prompted extensive studies involving both peptide design and spectral analyses.[26,28–42] For a turn-focused study, hairpins have the disadvantage that most of the residues in the peptide are not in the turn (yet contribute to spectral overlap, thereby obscuring the turn contribution), and those in the termini (which are open and frayed) often have considerable fluctuation.

Another option for turn modeling is to form small cyclic peptides, where the turn is constrained by the rest of the peptide or by another linker acting as a bridge.[24,25,43,44] One approach to this would be to make disulfide linked sequences,[45–50] and another has been to use mimetics.[24,51–55] A cyclic peptide is also constrained, and can form β-turns or other structures, depending on sequence and ring size. While large cyclic peptides can form a closed hairpin with designed turns, the problem of sorting out spectral responses arises when many of the residues have conformations other than that of the targeted turn.[36,56,57] Cyclic pentapeptides tend to form γ-turns with β-turns, somewhat mixing up the picture.[58] On the other hand cyclic hexapeptides can form more symmetrical structures with one cross-strand H-bond plus two β-turns or loops which may or may not close to form additional cross-strand H-bonds.[25,59–62] Many of these have been characterized and offer an opportunity to determine characteristic turn spectral behavior in a constrained environment and with minimal interference from "extra" residues.

One of the best ways for the detailed interpretation of peptide vibrational spectra is via density functional theory (DFT)-based computations. For large molecular systems these pose a difficulty since such computations become too large and added approximations must be made. We have had great success modeling spectra for regular structures by focusing on local interactions.[9,13,17,32,40,63,64] However in a cyclic or turn structure, the local interactions can be separated in a sequence due to cross-strand interactions. This has required us to develop methods of transferring properties obtained with computations for smaller molecules onto larger ones to obtain force field (FF), atomic polar and axial tensor (APT and AAT) values to determine IR and VCD frequencies and intensities.[40,65,66] An extension of this method has proven to be useful for simulation of the Raman and ROA spectra as well.[67,68] On the other hand, with current computational capabilities, a cyclic hexapeptide is small enough that we can do a complete FF, APT, and AAT computation, even including side chains. It is also an appropriate structure for extended MD trajectory calculations to explore conformational variations that can occur at different temperatures. Because of the cyclic constraints, these still result in a limited ensemble of conformations, which in turn can provide the basis for ab initio computations of their spectral properties.

Thus, to pursue such tests of peptide conformation—spectroscopic property correlation, we have chosen a cyclic peptide, c(FpGRGD), where p = ^{D}Pro, whose sequence suggests (based on previous NMR results) that stable Type II′ turn geometries will be formed.[62] We have explored the conformational space of this peptide with MD calculations at various temperatures and with different solvents and states of ionization (pH). We have simulated the spectra at the full DFT level for several model structures using both an all atom approach and a "stripped" structure where residues other than Pro and Gly (i.e. R,D,F) are substituted with Ala. This has allowed us to look at the effects of the fluctuation in the trajectory on the spectral results. These we then compared with experimental spectra of compounds we have synthesized. Use of such a limited size model system of restricted conformation has made possible the combination of MD and QM approaches without resorting to the transfer methods we have employed for larger peptides.

EXPERIMENTAL AND THEORETICAL METHODS

Peptide Synthesis

The c(FpGRGD) peptide was synthesized on an ABI Pioneer Peptide Synthesizer according to the manufacturer's protocols for the synthesis of backbone cyclized peptides. These protocols take advantage of three-dimensional orthogonal protection schemes[69] based on base-labile Fmoc, acid-labile (TFA) side-chain group, and allyl (Al) groups, which are piperidine and TFA-stable and removed with Pd(0) catalysts. This scheme for on-resin

synthesis of backbone amide and side-chain amide cyclized peptides was first systematically described by Barany and coworkers.[70] In this case, side-chain anchoring is desired to allow for on-resin backbone cyclization. For this sequence, anchoring is most conveniently offered through the side-chain of Asp, i.e., Fmoc-Asp(OH)-OAl is attached to an Wang-type linker (PAC-PEG-PS; commercially available from ABI) to provide the starting point for this synthesis. Coupling of the remaining residues utilized four equivalents each of Fmoc-protected amino acid (e.g., Fmoc-Arg(Pbf)-OH), TBTU, and HOBt (final concentration of each = 0.25 M) dissolved in 0.5 M DIEA in DMF for 1 h. On-resin cyclization was accomplished by first removing the final F_{moc}-group from the Phe-residue and then cleaving the allyl ester of the C-terminal Asp with a two-fold excess of $(Ph_3P)_4Pd$ in a solution containing 5% acetic acid and 2.5% *N*-methylmorpholine in $CHCl_3$. The allyl cleavage solution is recycled for 2 h and then the resin is washed with a solution of 5% DIEA and 0.5% sodium diethyldithiocarbamate in DMF to remove trace metal ions. The backbone amide bond formation between the amino group of Phe and carboxyl of Asp was accomplished with a four-fold excess of PyAOP dissolved in 0.5 M DIEA in DMF. PyAOP is utilized here to prevent guanidylation of the amino group which can occur with amidine-based coupling agents like TBTU and HATU.[71]

Experimental Spectroscopy

IR spectra were measured with a Digilab FTS-60A FTIR spectrometer (Varian, Randolf, MA) and VCD with a dispersive instrument developed at UIC and described extensively in the literature.[72] Samples were prepared by dissolving the cyclic peptide in D_2O with 0.1 M DCl and lyophilizing (twice) to eliminate TFA and redissolving (~45 mg/ml in D_2O, pH = 2). Alternatively, samples were dissolved without exchange in TFE or DMSO-d6 (~46 mg/ml) or with exchange in TFE-OD. The solutions were placed in cells composed of two CaF_2 windows separated by a Teflon spacer (50 or 100 μm), which were clamped in a brass ring and placed in a temperature-controlled holder of our own design.

Comparative ATR-IR spectra of dried peptide films deposited from H_2O and from D_2O were measured to encompass a wider spectral region. Samples were originally prepared at pH = ~2.6 or ~7.0 (to obtain spectra with contributions of either protonated and deprotonated Asp sidechains) by dissolving lyophilized peptide in H_2O or D_2O, then 7.5 μl was deposited onto the ATR crystal surface, and dried under N_2 flow. IR spectra were obtained at room temperature using a Pike Miracle ATR (3 bounce, ZnSe) and the internal DTGS detector by averaging 128 scans. Conversion to absorbance was done by referencing to an empty ATR cell.

For comparison, fluorescence and CD spectra (in the UV region) were obtained with a J-Y Fluoromax 3 and a JASCO J-815 dichrometer, respectively. Temperature for CD measurements was varied by flow from a Neslab RT-7 bath through a sample holder under instrument control.

Molecular Dynamics Conformational Studies

We initially performed test MD computations on a protonated variant of the cyclic peptide (i.e. with the Asp—COOH and Arg—$NHC(NH_2)_2^+$ side chains) as well as on the zwitterionic form (with Asp —CO_2^- and $NHC(NH_2)_2^+$). The protonated form is relevant to many of our experimental conditions and thus is analyzed in detail. The Amber 8.0, Gromacs (www.gromacs.org/) and Tinker programs were used for MD simulations.[73] General conformational behavior was explored with the Amber99[74] and OPLS-AA force fields in large solvent boxes (32 Å with Amber 8.0, zwitterion in H_2O and DMSO, 40 Å with Gromacs for the protonated form in H_2O), where several MD runs of 10–60 nsec were performed. The common TIP3P water[75] and OPLS-AA TFE force field were used with a particle-mesh Ewald (PME) summation.

Simulated annealing was run with Tinker software using an Amber 99 force field (from 1000 to 300 K) for the protonated form and was followed by running short MD trajectories at 300 K with the same FF. From these trajectories, 10 MD configurations were selected for ab initio computation, by sampling every 100 psec from a 1 ns trajectory, run at 300 K, NpT ensemble, with 1 fsec time steps. MD computations were realized on various Linux-based computers.

Ab Initio Vibrational Spectral Computations

Selected conformations from the MD trajectories above were used for DFT determinations of vibrational spectroscopic properties, calculated with the Gaussian 03 software package.[76] Some conformers were fully optimized, but for most of them a constrained normal mode optimization method[77,78] was used to retain the MD conformation by fixing coordinates for modes less than 300 cm^{-1}. In this way, the higher-frequency modes, presumably important for the spectra, could be relaxed while having a minimal impact on the MD determined conformation (primarily dependent on low frequency torsional modes, Figure 1). For optimized structures the force fields (FF), atomic polar and axial tensors (AAT, APT) were calculated. In most cases the BPW91/6-31G** functional and basis set was used with the COSMO solvent correction (exceptions will be noted). Some of the DFT computations were simplified by reducing the R (Arg), D (Asp), and F (Phe) side chains to $—CH_3$, i.e. substituting with Ala, but retaining G (Gly) and P (Pro) residues, which enabled DFT exploration of amide spectral features, which are of prime interest to the IR and VCD, for more conformations with alternate structures. Also some tests were done on a fully Gly substituted sequence ($cGly_6$) whose conformation was constrained to one set of MD determined ϕ, ψ values. Additionally, computations to determine optimal methods were performed on the $cGly_6$ model peptide in vacuum with the B3LYP/6-31G** to test the impact of using a hybrid functional and with BPW91/6-311++G** to test the effect of a basis set containing diffuse functions. While DFT calculations for cyclic model peptides without side chains could be calculated on a Linux cluster with 32-bit/2GB nodes, computations on hexapeptides with full side chain representations

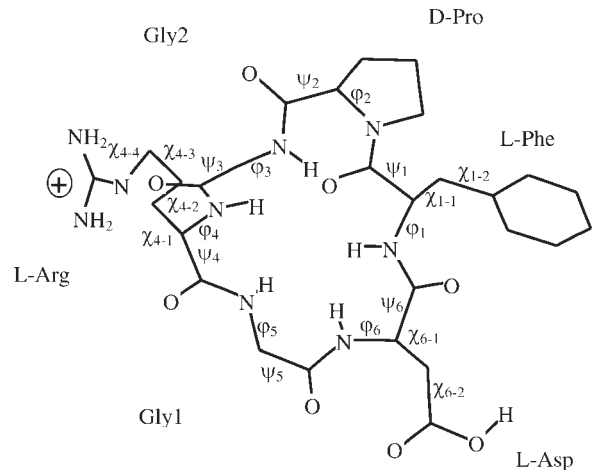

Fig. 1. Definition of the c(FpGRGD) cyclic hexapeptide torsion angles and numbering scheme.

were run on 64-bit PCs with up to 16 GB RAM. Simulated spectra of both protonated and deuterated peptides were generated with these DFT-level parameters using our own supplementary programs.

RESULTS

Experimental Spectral Data

ECD (electronic circular dichroism in the UV range) spectra were measured for the peptide in H_2O and TFE at neutral and acidic pH. The spectra (shown in Fig. 2) have a negative broad feature with a minimum at ~202 nm which while not characteristic of any standard model peptide secondary structure, presumably reflects the turn geometry modified by the Phe-^{D}Pro-Gly linkage. The pattern is roughly similar to that seen by Vass et al.[25] in their study of similar cyclic peptides, in which it was recognized that although the CD resembled that of a disordered structure, that could not be correct (since it is cyclic). They also noted this CD is not typical of known β-turns and thus might be more complex due to conformational averaging. This suggestion is further supported by the CD bands we have reported for the NG4 and ^{D}PG4 peptides (Ac-VNGK-NH_2, disordered, and Ac-^{D}PNGK-NH_2, Type I′ turn, respectively) being of the opposite sign.[38] There is little effect of acidic pH on the spectra, but the TFE data did have an extra negative band at ~193 nm. Similarly, the fluorescence of this cyclic peptide with either 250 or 280 nm excitation, while different, is similar in both solvents, but in TFE is much broader, suggesting some quenching mechanism (data not shown).

IR and VCD spectra were measured for the cyclic peptide in D_2O, TFE-OH, TFE-OD and DMSO, at different pH values, and ATR-IR spectra were measured on dried films taken from H_2O and D_2O solutions at high and low pH, to obtain both protonated and H/D exchanged samples and to observe the effects of protonation of the Asp side chain. Because of its small size and nonregular geometry, the Phe-^{D}Pro linkage, and the Asp and Arg side chains, this cyclic peptide gives rise to several partially resolved bands in the amide I region that may (at some level) be associated with local modes. The positions and relative intensities of these are sensitive to pH, and the TFE results to H/D exchange. The solution phase IR spectra are broader in D_2O than in the organic solvents, but accounting for the linewidth differences, the D_2O and TFE data are consistent, but are shifted in frequency with D_2O being lower (Table 1 and Fig. 3, where the D_2O and TFE results are compared). The DMSO and TFE-OD data are not shown.

Again allowing for frequency shift and line broadening, and correcting for some variation in baseline, the VCD spectra of all three solution phase samples have the same fundamental coupled oscillator-like (alternating sign sequence) VCD pattern. Within the amide I profile, a dominant strong couplet appears, which is correlated to the higher wavenumber absorption component. The bandshape is negative then positive with decreasing frequency (at 1671 and 1647 cm^{-1}, respectively, in D_2O, while in TFE the corresponding negative band has two components at 1692 and 1680 cm^{-1} and the positive band is at 1651 cm^{-1}). Typically a weaker nega-

TABLE 1. Comparison of observed amide I frequencies and intensities for c(FpGRGD) in D_2O and TFE

D_2O				TFE			
IR		VCD		IR		VCD	
Frequency (cm^{-1})	Intensity (A)	Frequency (cm^{-1})	Intensity (10^{-5} ΔA)	Frequency (cm^{-1})	Intensity (A)	Frequency (cm^{-1})	Intensity (10^{-5} ΔA)
1710[a]	0.09	1701	0.1	1725[a]	0.08		
		1671	−1.1			1692	−1.9
1648	0.40	1647	1.8	1674	0.78	1680	−2.0
						1651	3.5
1622	0.38	1622	−0.4	1634	0.56	1632	(–)[c]
1587	0.16	1601	8.4			1631	1.0
				1530[b]	0.22	1523[b]	2.5

[a]Mostly due to Asp−COOH.
[b]Amide II band in TFE−OH.
[c]Negative band between two positives.

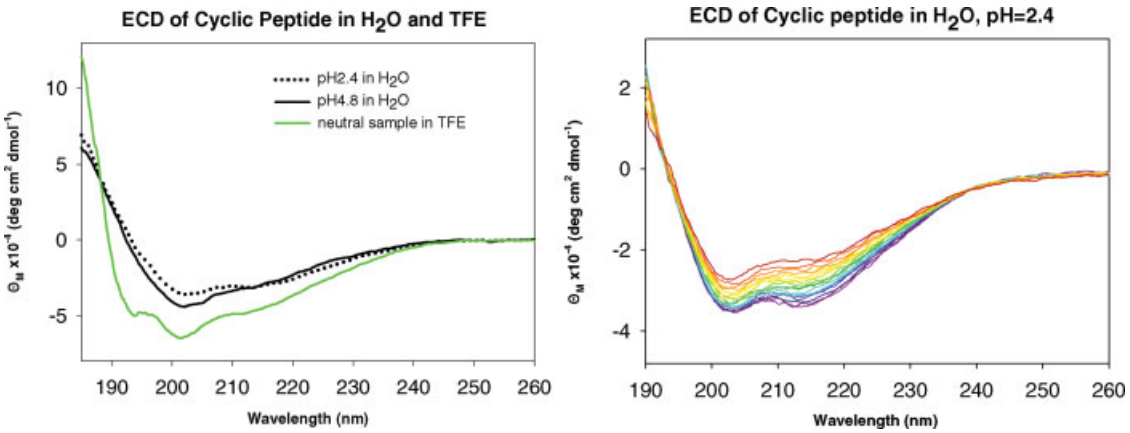

Fig. 2. ECD spectra of the c(FpGRGD) hexapeptide in H_2O at low (dotted line) and neutral pH (black solid line) and in TFE (green line) at room temperature (left) and in H_2O (acidic pH) from 5 to 85°C (right), where violet/blue (more intense) are the low temperatures and orange/red the hot. [Color figure can be viewed in the online issues, which is available at www.interscience.wiley.com.]

tive and positive VCD are seen to the low wavenumber side of the amide I, with the negative component corresponding to the prominent lower wavenumber absorption band (Table 1 and Fig. 3, right side).

The ATR-IR for low pH samples (see Fig. 4) has an amide I band with a maximum at ~1625 cm^{-1} and a shoulder at ~1650 cm^{-1}, which are altered in relative intensity from the solution phase data. They also show a broad amide II band at ~1525 cm^{-1} that shifts to ~1450 cm^{-1} on H/D exchange. A presumed amide III band occurs at ~1280 cm^{-1} but is quite dispersed and obscured by overlap with side-chain modes (as evident from comparison of H_2O and D_2O spectra, see inserts in Fig. 4). At neutral pH, the Asp—COO^- band gives a broad band from 1530–1580 cm^{-1} and at low pH the Asp—COOH is at ~1710 cm^{-1}.

MD-Derived Geometry

The torsional angles for the definition of the cyclic peptide conformation are defined in Figure 1. For VCD and IR, the backbone conformation is most relevant and will be the focus of the discussion in this article. While side chain conformational fluctuations were also analyzed, they are most relevant for Raman spectral studies, which will be discussed separately with relevant experimental data and Raman simulations.

An overall equilibrium between conformations could only be sampled with MD using relatively long time simulations. Important conformational transitions such as the flipping motion of the ^{D}Pro-Gly turn between Type I′ and II′ turns could only be observed, even for 100 nsec runs, with higher temperatures and certain force fields. In particular, Amber99 showed no transitions from conformations started having a Type I′ turn, but OPLS led to conformers with Type II′-like turns at long times. Only by use of high temperature simulations could such transitions be revealed in the MD trajectories. In Figure 5a, the time dependent conformational fluctuations showing such a transition are illustrated in terms of changes in the radius of gyration (R_g) and dihedral angles sampled during a trajectory obtained at 450 K. While the R_g does not vary drastically, as would be expected for a cyclic molecule, the Pro dihedral angles, ϕ_2, ψ_2, have a sharp transition in ψ_2 from ~0° to ~ −130° and back during the 14 nsec trajectory (Fig. 5b). This is consistent with a change from approximately Type I′ to II′ for the Pro-Gly turn. More or less concerted with that change is a flip of the Gly5 ϕ_5 from 110°

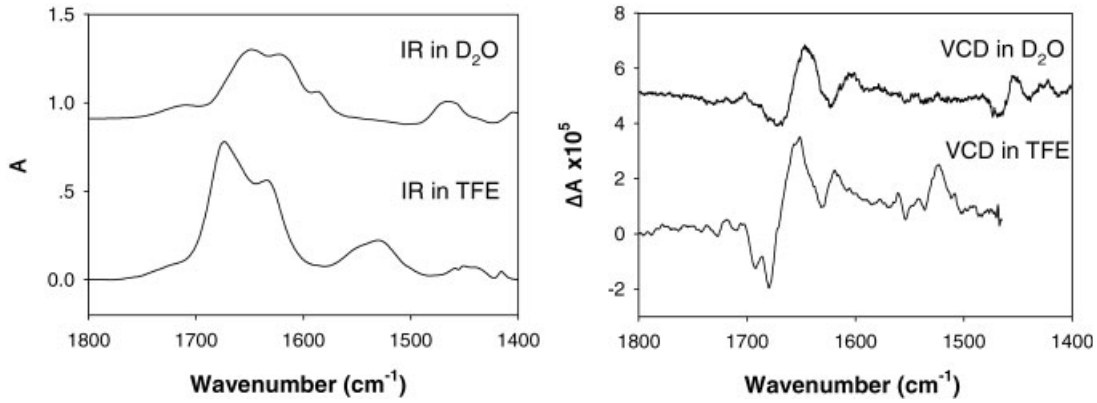

Fig. 3. Experimentally obtained IR (left) and VCD (right) spectra of the c(FpGRGD) hexapeptide in (top) D_2O (pH = 2) and (bottom) TFE.

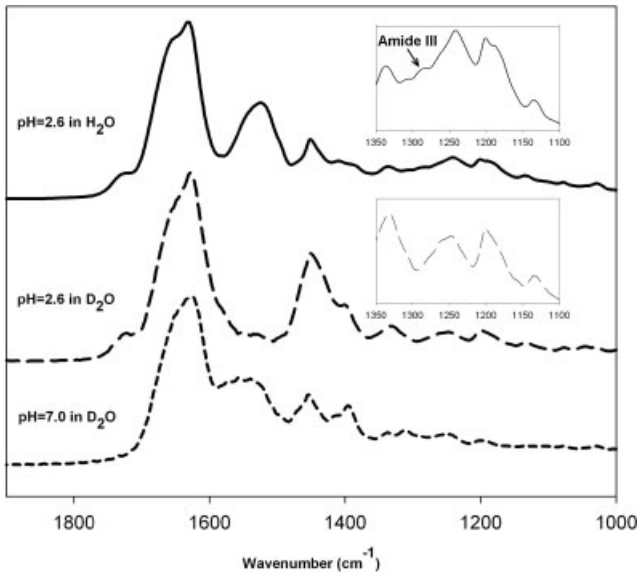

Fig. 4. ATR-IR spectra for films of the c(FpGRGD) peptide deposited from H_2O (top, solid line) or D_2O at pH 2.6 (middle, dashed) or 7.0 (bottom, short dash). Inserts show expanded amide III regions.

to -140°, but the ψ_5 value is more variable, indicating that this turn has a less well-defined conformation (Fig. 5c).

Figure 6 shows the corresponding distributions of dihedral angles derived from the same trajectory for each residue, F1,p2,G3,R4,G5,D6 in the order Figures 6a–6f, respectively. Overall, the observed conformational fluctuations suggest that this cyclic peptide has stable mixed structures most often composed of two turns and a (very short) anti-parallel β-strand structure. The two turns are achieved in the ^{D}Pro2-Gly3 sequence (numbering as in Fig. 1), with the dihedral angles corresponding to the ^{D}Pro2 and the Gly3 residues being close to values expected for tight β-turn Type I′ ($\phi_2\sim60$, $\psi_2\sim30$, $\phi_3\sim90$ and $\psi_3\sim0^\circ$) or Type II′ ($\phi_2\sim60$, $\psi_2\sim-120$, $\phi_3\sim-80$ and $\psi_3\sim0^\circ$) values. The other turn, composed of the Gly5-Asp6 residues, is quite distorted from these ideal values, but may also have two dominant conformational populations. However, they are not β-turns, in that three N—H groups (F1,D6,G5) tend to point in toward the center of the turn, rather than forming a H-bond with a C=O. Two residues, Phe1 and Arg4, form an elemental anti-parallel sheet structure, but as seen in Figure 5d, both cross-strand H-bonds are infrequently formed, presumably due to the distortion at the second, non-β-like turn (Gly5-Asp6). In particular, the dihedral angles of the Phe1 residue are consistent with an anti-parallel β-strand structure (Fig. 6a), but the Arg4 has a broader distribution in ψ.

The MD-derived structures described above are consistent with the results of our simulated annealing calculations (see below) which also converged on a cyclic structure with a Type I′ turn and a distorted, non-H-bonded turn at the Gly-Asp end. The MD results show a definite dispersion in the structures the ring can achieve, but also imply substantial barriers between them. The question remains if the structures can be discriminated or the equilibrium studied spectroscopically. This is a challenge for the QM spectral simulations.

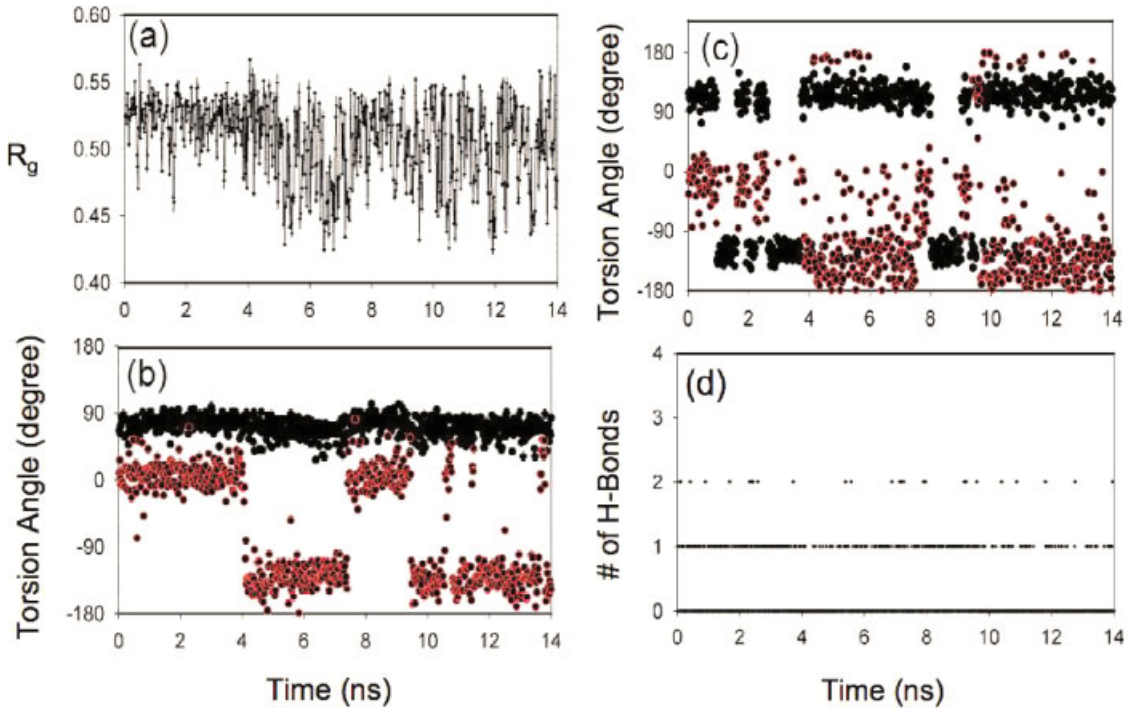

Fig. 5. Time-dependent equilibrium conformational fluctuation. MD trajectory carried out at 450 K with a total simulation time 14 nsec illustrating changes in the: (**a**) radius of gyration (R_g) of the entire peptide; (**b**) dihedral angles (ϕ_2 = black, upper, single value trace, ψ_2 = red) of the ^{D}Pro residue in the ^{D}Pro-Gly turn; (**c**) dihedral angles (ϕ_5 = black, mostly upper trace, ψ_2 = red) of the Gly5 residue in the Gly-Asp turn; and (**d**) number of H-bonds among the backbone amide groups. [Color figure can be viewed in the online issue, which is available at www.interscience.wiley.com.]

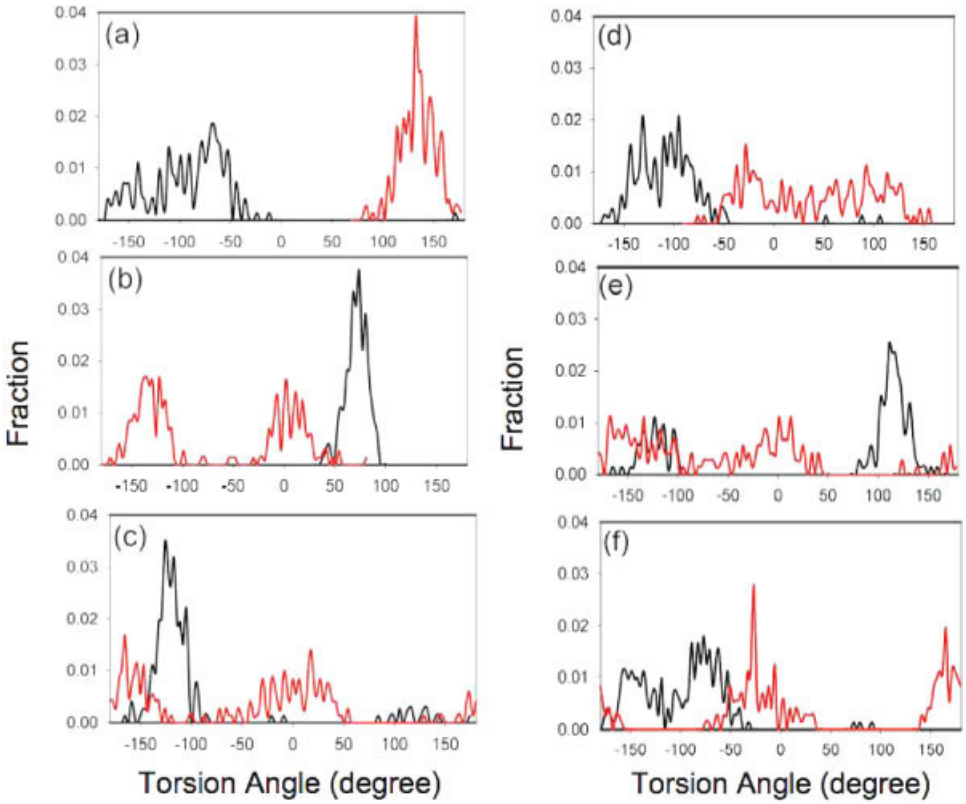

Fig. 6. Relative distribution of dihedral angles of each residue in the same 450 K trajectory as Figure 5. Values indicate fraction of population distribution in a degree. The black line is for ϕ, and the red line is for ψ. Residues are: (**a**) Phe1, $\phi \sim -70$ to -150, (**b**) DPro2, $\phi \sim 80$, (**c**) Gly3, $\phi \sim -120$, (**d**) Arg4, $\phi \sim -100$ to -130, (**e**) Gly5, $\phi \sim 120$ and -120, (**f**) Asp6, $\phi \sim -80$ and -150. [Color figure can be viewed in the online issue, which is available at www.interscience.wiley.com.]

Simulated Annealing

The conformational distributions evident in the MD runs described above indicate typical structures to select for further study. The equilibrium obtained for the peptide backbone geometry conformation by simulated annealing with the Amber99 force field was conserved at 300 K, but the side-chain conformations varied widely. The torsion angles (defined in Fig. 1) of the main cyclic peptide chain for a 1 nsec MD trajectory subsequent to the annealing had rms deviations within 9–17° of the average values as summarized in Table 2. Not surprisingly, the Gly residue moved most ($\Delta\tau \sim 15°$) while the flexibilities of the other residues were smaller, $\Delta\tau \sim 10$–$13°$; the most rigid being the proline residue. The peptide backbone flexibility appears to be moderated by the side chain characteristics. The cyclic peptide thus again resembles two Type I′ β-turns, one induced by the Pro-Gly, while the charged amino acids partially stabilize the structure by formation of intramolecular hydrogen bond bridges.

The MD trajectories were influenced by the starting geometry and the computational scheme, presumably due to the constraints of the ring, which can lock the peptide into a local minimum for a considerable time at low temperatures. High temperature simulations show that rapid transitions between Type II′ and I′ turns are possible (see Fig. 5b) if one uses a cutoff for long range interaction correc-

TABLE 2. Average torsional angles and their dispersion obtained from simulated annealing

Backbone	*F*		*P*		*G*		*R*		*G*		*D*	
Torsion[a]	ϕ_1	ψ_1	ϕ_2	ψ_2	ϕ_3	ψ_3	ϕ_4	ψ_4	ϕ_5	ψ_5	ϕ_6	ψ_6
$<\tau>$	−141	157	62	16	74	20	−134	10	168	−56	−136	−21
$<\Delta\tau>$	9	9	10	11	15	15	13	12	12	17	13	14
Sidechain	*F*		*R*				*D*					
Torsion	$\chi_{1\text{-}1}$	$\chi_{1\text{-}2}$	$\chi_{4\text{-}1}$	$\chi_{4\text{-}2}$	$\chi_{4\text{-}3}$	$\chi_{4\text{-}4}$	$\chi_{6\text{-}1}$	$\chi_{6\text{-}2}$				
$<\tau>$	−97	98	68	−175	−68	−179	−62	−84				
$<\Delta\tau>$	12	14	9	22	9	45	13	17				

[a] $<\tau>$, average torsional value; $<\Delta\tau>$, root mean square deviation.

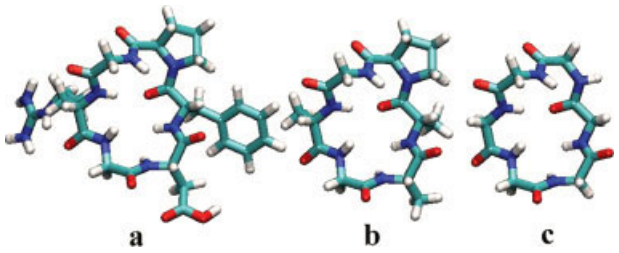

Fig. 7. Geometry of the full c(FpGRGD) peptide in a Type I′ turn form (**a**, left), its "alanine" (**b**, middle) and "all-glycine" (**c**, right) analogues taken for the spectra computations (based on the A-4 conformer of Table 2). [Color figure can be viewed in the online issue, which is available at www.interscience.wiley.com.]

tions. Simulated annealing can overcome these relatively large barriers to conformational transition, making the resulting structures a reasonable representation for the solution structure. Since we have chosen to employ ^{D}Pro-Gly to stabilize one turn, it is not surprising that the structures differ from previously determined cyclic hexapeptide NMR results. The force fields chosen for our simulations probably also contribute to the deviation.

Quantum Mechanical Spectral Modeling

For spectral modeling we randomly selected 10 MD peptide geometries (A1-10) from a 1 nsec Tinker/Amber simulation of the positively charged form. These structures all had an approximate Type I′ turn at the ^{D}Pro-Gly residues plus the distorted tight loop characteristic of the highly annealed sample. Graphical representations of a typical version of the Type I′ containing structure (A-series) are shown in Figure 7, with and without side chains. To give some idea of the consistency of the ring backbone conformation and the variation of the sidechains, we plotted an overlapped version of these 10 structures in Figure 8a. These structures were partially DFT optimized at the BPW91/6-31G** level with a COSMO representation of the solvent and with constraints along normal coordinates for modes <300 cm^{-1}.[77,78] Final torsion angles for this set are given in Table 3 (columns labeled A1–A10).

The alternate turn conformation did not occur during this short MD run, thus to provide a comparison, four Type II′ conformers (B-series) were constructed from an MD simulation of the zwitterionic state (structures B1–B4 in Table 3). Use of the MD structures with restricted COSMO optimization resulted in more separation of the cross-strand parts of the B-type ring, so that while the N—H and C=O remained directed at each other; the distances became too large for H-bonding. Thus the solvent corrected QM structure and the MD in solution structures are related in having weaker (longer) cross-strand H-bonds. If these B structures were instead fully optimized in vacuum without constraint, the H-bonds were formed, i.e. the ring tightened up on itself, and systematic changes in ϕ, ψ angles are clear. For the A structures, such a contraction is not seen, and the vacuum structures and ϕ, ψ angles are similar to the COSMO structures, which may be due to the unusual loop formed at the Gly5-Asp6 segment which cannot form an H-bond. Two examples of full minimization in vacuum are indicated as B-1_{vac} and A-4_{vac} in Table 3. As is clear from Table 3, the variation in the ϕ, ψ angles for the respective Type II′ and I′ conformations is not large among these selected conformations and we thus expect their spectra to be relatively consistent for the amide modes. Surprisingly, in Figure 8, the overlaid A structures show more variation at the ^{D}Pro-Gly Type I′ turn end than the other end, while the B structures are more closely overlapped on both ends. This is not evident in the Table 3 comparison and probably indicates a coupling of different motions to relax the molecules, which could be symptomatic of convergence to a multiple minimum. However the change between Type I′ and II′ turns, i.e. between the A and B series, is substantial and affects all of the torsion angles, indicating that change is global. The question remains as to its impact on spectra.

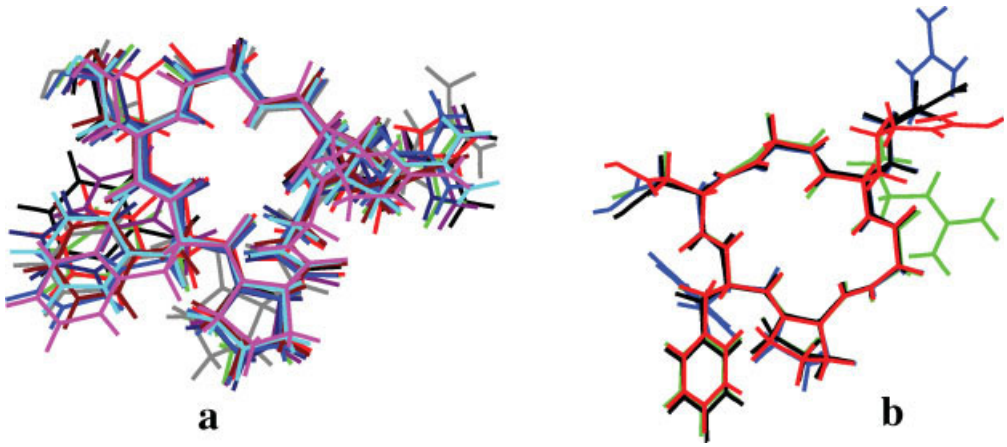

Fig. 8. For the c(FpGRGD) peptide, overlap of (**a**-left) 10 structures derived from a 1 nsec MD trajectory after simulated annealing (A1-10, Table 3) which maintain a Type I′ turn at the ^{D}Pro-Gly linkage and (**b**-right) four structures (B1-4) which have a Type II′ turn on both ends (^{D}Pro-Gly and Gly-Asp) and potential (but long) anti-parallel cross-strand H-bonds. [Color figure can be viewed in the online issue, which is available at www.interscience.wiley.com.]

TABLE 3. Torsion angles of c(FpGRGD) MD conformations selected for ab initio computations

	Type II′ turns				Type I′ turns										Vacuum	
τ	B-1	B-2	B-3	B-4	A-1	A-2	A-3	A-4	A-5	A-6	A-7	A-8	A-9	A-10	A-4$_{vac}$	B-1$_{vac}$
ϕ_1	−153	−137	−145	–154	−126	−148	−143	−139	−133	−141	−146	−144	−143	−146	−132	−113
ψ_1	130	132	159	125	165	132	163	156	170	156	160	160	153	169	152	101
ϕ_2	73	81	71	79	57	63	56	52	74	47	46	65	62	73	53	65
ψ_2	−142	−143	−151	–139	25	28	19	23	15	12	30	11	9	16	24	−107
ϕ_3	−93	−86	−85	−84	59	60	66	70	69	92	39	66	92	78	72	−109
ψ_3	−10	−22	−23	−19	13	39	39	35	16	18	60	33	37	14	33	20
ϕ_4	−143	−148	−146	–150	−124	−153	−145	−145	−138	−141	−143	−138	−168	−143	−144	−148
ψ_4	120	121	118	156	9	20	13	7	3	20	−6	10	3	−10	10	118
ϕ_5	92	103	109	82	178	173	160	−170	164	161	171	168	−179	−177	−174	70
ψ_5	−134	−144	−146	–135	−71	−73	−61	−58	−23	−51	−27	−67	−76	−47	−55	−129
ϕ_6	−111	−95	−91	–114	−132	−151	−127	−132	−153	−143	−146	−126	−132	−130	−137	−101
ψ_6	16	−12	−12	12	−27	6	−32	−22	−44	−15	−29	−28	−15	−35	−25	13

Peptide Vibrational Modes

The amide mode frequencies are sensitive to the basis set and functional approximation used. In order to evaluate the impact of this variance, and to determine an appropriate level for pursuing our various cyclic peptide computations, we arbitrarily chose a single structure and did a number of test computations varying the approximations used. For the model in Figure 7c, where all residues are substituted by Gly, but the ϕ, ψ torsional angles of A-4 in Table 3 were maintained, IR and VCD were computed at the B3LYP/6-31G**, BPW91/6-31G** and BPW91/6-311++G** levels, all with the COSMO solvent correction, and are compared in Figure 9. The relative IR intensities and VCD band shapes of the main amide bands are conserved for all levels of theory used, but their frequencies show a steady decrease for this variation of DFT methods, which is most distinct for the amide I, as expected. There are differences in the hybrid (B3LYP) functional results including a band at ~1350 cm^{-1}, but there are few IR or VCD data for comparison with these predictions especially since the side chains will dominate this region for real systems. Such considerations can be important for the Raman interpretations, which will be considered separately.

The most important characteristic, the amide I-II gap is also reduced by changing from the hybrid functional (B3LYP, where the gap is ~220 cm^{-1}) to BPW91, and even further by use of the diffuse orbitals (6-31++G**) bringing the average amide I–II separation down to ~140 cm^{-1} in (Fig. 9c), which approaches the experimental value of ~100 cm^{-1}. (It should be noted that, without inclusion of explicit solvent, we would not expect to achieve the experimental amide I-II separation value in our DFT-based simulations.[17,21,79]) The B3LYP functional contains the Hartree-Fock exchange term and is computationally somewhat slower than BPW91, which thus costs more time and offers no advantage (actually poses a disadvantage) for these amide centered modes of prime consideration in peptide IR and VCD spectra. Although the results are better, computations with the basis set containing the diffuse functions (++) are much slower than with 6-31G**, which can become prohibitive for realizing calculations with larger peptides. For example, with the cGly$_6$

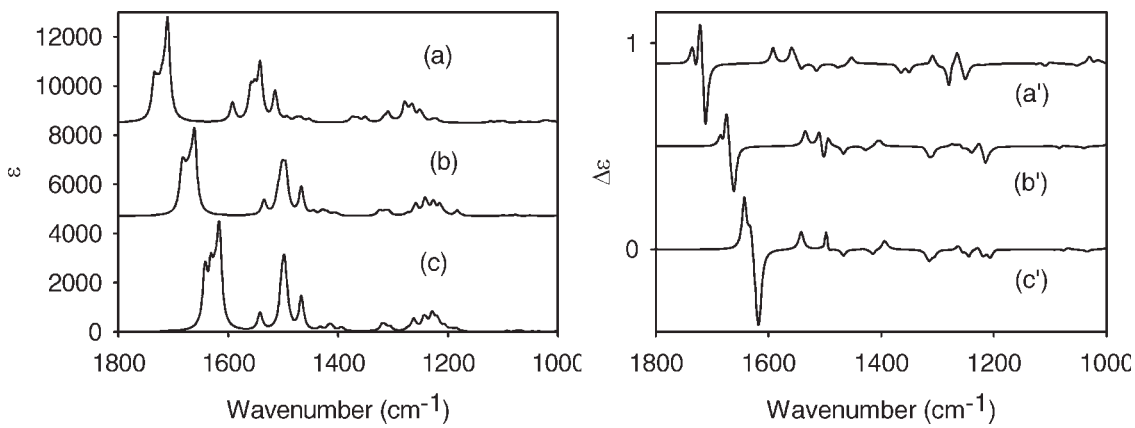

Fig. 9. Absorption (left) and VCD (right) spectra of the glycine analogue of the c(FpGRGD) peptide, cGly$_6$, simulated for the A-4 conformation at the B3LYP/COSMO/6-31G**(**a**,**a**′), BPW91/COSMO/6-31G** (**b**,**b**′), and BPW91/COSMO/6-311++G** (**c**,**c**′) levels.

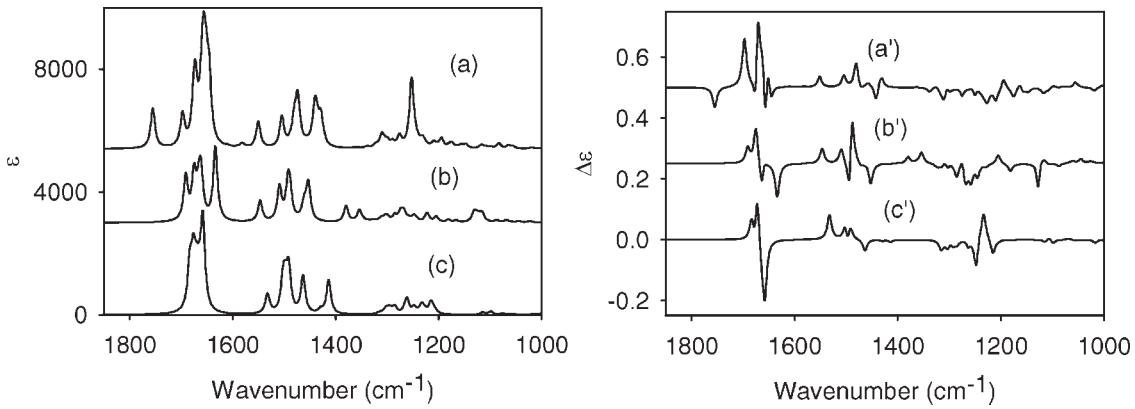

Fig. 10. Comparison of absorption (left) and VCD (right) spectra simulated for the full c(FpGRGD) peptide (**a**,**a**′) and its Ala-like, c(ApGAGA), (**b**,**b**′) and glycine, $cGly_6$, (**c**,**c**′) derivatives at the BPW91/COSMO/6-31G** level. See Figure 7 for the respective geometries. For (c,c′) the glycine CH_2 were Cα H/D exchanged to form L-d_1Gly. These results can be compared to the experimental IR and VCD data in Figure 3.

peptide, addition of diffuse functions expanded the basis set by ~50% and the time for the frequency calculation increased fivefold on our computers. Since the relative dispersion and intensity patterns found with 6-31++G** level computations are preserved in both the IR and VCD spectra with the smaller basis set, we consider the BPW91/6-31G** method to be an acceptable compromise that allows us to compute larger peptide systems and qualitatively estimate the impact of factors, such as structure, flexibility and molecular environment. Detailed mixing of local modes does vary somewhat yielding small differences in quantitative mode intensities, but a consistent qualitative pattern is maintained, which results in very similar overall IR and VCD amide I and II bandshapes. Since the general basis set dependent patterns are established, we can incorporate reasonable corrections for known frequency error systematics (diagonal FF elements), if it is desired to better align predictions with the experimentally observed dispersion. Furthermore, since it is established that the solvation effects are the main error in these computed frequencies, the virtue of basis set expansion without solvent correction is debatable.[68,79–81]

Since the BPW91/COSMO/6-31G** calculational level is seen to be most efficient for the targeted amide modes, a series of computations were then directed at modeling the impact of the side chains on the spectral shapes. We compared the DFT computed spectra of the whole peptide (including side chains) with that of its Ala analogue, c(ApGAGA),where side chains, except for Pro and Gly, were replaced by $-CH_3$, and finally with the simplified $cGly_6$ analogue (as illustrated in Figure 7). The A-4 conformation was again arbitrarily selected for these tests. We chose a specific conformer, because, while the angles in Table 1 represent the average geometry well, they cannot yield a realistic geometry since the angles were averaged independently. IR and VCD spectra computed for the three cyclic peptide analogues (Figs. 7a–7c) are thus plotted in Figures 10a–10c. Using the $cGly_6$ spectra (Figs. 10c and 10c′) as a reference, we can assess the impact of the side chain perturbations on the amide I, II, and III vibrations. Since the Gly CH_2 group scissor motion overlaps the amide II in this DFT-derived FF (vacuum), the molecule was modified to be pseudo chiral by changing the mass of the appropriate H to 2, i.e. H/D exchange yielding the L-d_1-Gly variant, thereby modifying the scissor mode into a C_α—H (and C_α—D) wag that would be normally present in these residues. The impact of this correction was relatively small, as can be seen by comparing Figures 9b and 9b′ with Figures 10c and 10c′.

For $cGly_6$, the amide I mode spectrum has the least dispersion for the three structures used in this comparison, and less than seen experimentally, having a computed maximum at 1662 cm^{-1} and shoulder at 1680 cm^{-1}. Incorporating the D-Pro residue and substituting Ala for the other three non Gly residues (Fig. 7b) leads to splitting of the amide I band and development of a distinct low frequency component (computed at ~1632 cm^{-1}) due to the Phe1-Pro2 tertiary amide.[38] The amide I modes in the Ala-based peptide are relatively uncoupled, each assignable to a specific amide from G5 on the high frequency side to p2 then A6(D),G3,and A4(R) overlapped to A1(F), resulting in a dispersion perhaps slightly larger than seen experimentally. The amide II band also showed an increase in dispersion for the Ala model (Fig. 10b), which may correlate to its mixing with Ala—CH_3 modes and the Pro—CH_2 modes that are actually calculated as partially interspersed with the lowest amide II components. Amide III modes are also affected by the side chains and couple with the methyl motion as well as the C_α—H deformation. These frequencies are dispersed between 1205–1274 cm^{-1} in this model while the C_α—H bands are mostly higher, but their IR intensities are so low as to make the spectrum in this region non-descript, just a series of poorly resolved features spread over 100 cm^{-1}.

Finally, by incorporating realistic side chains (Fig. 10a) into the computation, distinct new modes are seen corresponding to the added functional groups. However, the amide I vibrations actually become less dispersed, and the amide I modes become more mixed, each assignable to 2 or more local amides. While the C=O stretching vibration of the Asp—COOH group is computed at 1756 cm^{-1}, the highest amide I component is again dominantly G5 with p2+R4 modes forming the next feature and F1 + D6 the

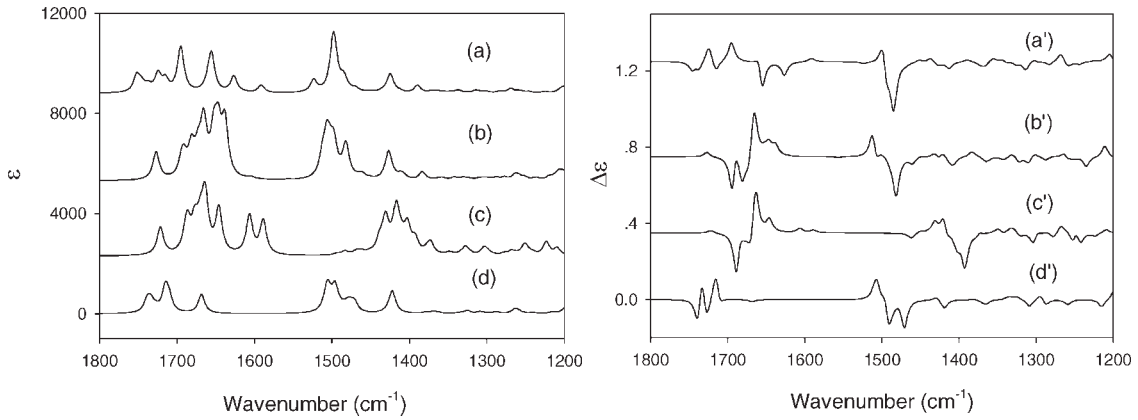

Fig. 11. Left—predicted IR spectra of the c(FpGRGD) B-1 conformer calculated with BPW91/6-31G* (**a**) in vacuum, (**b**) with COSMO, and (**c**) the full c(FpGRGD) peptide N-deuterated as compared to (**d**) for c(ApGAGA), Ala side chains only, in vacuum. Note that (a) and (d), the results in vacuum are in general alignment, if the absence of the Arg and Asp side chain contributions in c(ApGAGA) are taken in consideration. Right—the corresponding calculated VCD spectra, with (**a′–d′**) same conditions as on the left.

main peak. The Arg4 side chain vibrations are computed at ~1646–52 cm^{-1}, forming the low frequency shoulder on the amide I in Figure 10a, and these effectively push up the (Phe1-^{D}Pro2) amide frequencies. The amide II mode for the peptide with sidechains in (Fig. 10a) appears more dispersed but with the same intensity pattern as for the simplified models (Figs. 10b and 10c), even though it is highly overlapped with Phe and other $—CH_2$ based modes. Those side chain modes often have less dipole strength, so their impact on the IR is smaller making the observed pattern reflect the intensity dominance of the amide modes. Only highly dipolar side chains like Asp and Arg contribute to the IR at a level that is significant for single residues. However, the C—N stretch mode of the F1-p2 amide is computed at ~1420 cm^{-1} with relatively high dipole strength in most simulations. As noted above for the $cGly_6$, the amide III region does have most of its IR intensity from overlapping side chain modes, since it has only very weak amide vibrations. The computed full c(FpGRGD) spectrum has strong Asp side chain C—O—H bending (1253 cm^{-1}) and C—O stretching (1310 cm^{-1}) IR transitions in this region.

The VCD spectra (Figs. 10a′–10c′) differ more between the various side chain representations. However, some common patterns can be recognized, such as the dominant amide I negative couplet, distorted to a (+,+,−) pattern from high to low frequency for these A-type conformers. The lower negative band is stretched out due to the Phe1-Pro2 amide shift down in frequency for the Ala model (Fig. 10b′) and is further distorted by addition of the Arg4 overlap in the full side chain calculations (Fig. 10a′). The main difference in the amide I is that the overall positive couplet VCD which clearly dominates the spectra for the Gly and Ala models is obscured in the full calculation, where it apparently loses a negative component due to band overlap. In VCD simulations the chiral contributions of Arg4, Asp6, and Phe1 will be computationally overestimated, since in solution their side chains will sample many conformations, but these calculations necessarily select out just one of them. This plus the fact that they are also calculated to lie high in wavenumber (in both relative and absolute senses) means they interfere in the computational analysis of the amide I VCD spectrum. While the overall amide VCD pattern can still be determined from the full peptide calculations it does not adequately resemble the experimental one for the amide I.

The amide II VCD has more variation with the side chain approximation used, perhaps because amide II motion can be coupled to the methyl C-H bending modes, but remains net positive, while the amide III region has many broadly dispersed bands but is net negative. Either of these might agree with the experiment, but the data are too broad and weak to be certain. Dependence of the IR and VCD spectra on the side chains is often ignored, normally replacing them with methyls or hydrogens for QM spectral simulation.[12,38,82,83] Such an approach works well for homopeptides or for periodic peptide structures, such as sheets or helices, where the perturbations are uniform, thus leading to an overall shift of the spectrum maintaining relative relationships. Variable side chains can cause difficulty in modeling irregular cyclopeptide spectra,[40,66] but with careful assignment, their impact can be taken into account, since they mainly shift the amide frequencies, or serve to disperse the amide character among nearby modes, rather than change its nature or chirality.

Solvent Correction Model Comparison

After having assessed the role of the side chains we compared models for the effect of the solvent on the vibrational spectra. Fundamentally in all cases where we compare the same molecules with and without COSMO correction for solvent effects, the COSMO amide I results are shifted down in frequency and the dispersion is compressed as compared to vacuum (contrast Figs. 11a and 11b). That added dispersion (~150 cm^{-1}) in vacuum is accompanied by (at least partial) reversion to localized oscillator modes, which includes decoupling the Arg side chain modes from the amide I when the side chains are represented. (For the B-1 conformer, Arg modes are com-

puted at ~1655 cm^{-1} and 1695 cm^{-1} partially interspersed with the amide modes in vacuum but are lower in frequency and less dispersed using COSMO correction. In A-4, the relationship is different in detail but qualitatively the same, COSMO being lower than in vacuum, but there resulting in Arg side chain vibrations overlapping amide modes in both cases.) A similar decoupling, at least partially, of the amide I modes occurs on H/D exchange of the amide to yield the amide I′ modes, as can be seen in Figures 11b and 11c. While the dispersion does not change very much on *N*-deuteration, the Arg side chain modes shift down by ~50 cm^{-1}, and the amide pattern clarifies. This is commonly the situation that would be seen in peptides dissolved in D_2O.

To visualize these solvent effects, we changed our focus structure from that of the previous figures and plotted in Figure 11 the computed IR and VCD spectra for the B-1 conformer for c(FpGRGD) with all side chains included in (a) in vacuom and with COSMO, both (b) protonated and (c) *N*-deuterated and below that plotted (d) the computed spectra for the all Ala, c(ApGAGA), version (but again in vacuum) for the same ring geometry. With these computations for the B-ring geometry (two Type II′ turns), we can see some regularity. The highest mode is again the Asp—COOH, followed by the amide I modes whose highest component is the Pro amide, followed by mixtures of the D6, G5, and R4 amides with increasing intensity to the maximum intensity amide mode which is centered on the G3 amide, and finally a weaker F1 amide is shifted down in frequency (due to the Phe-^{D}Pro tertiary amide bond). Overlapping the F1 amide I are the Arg side chain modes which shift further down on deuteration and (partly) in vacuum, as noted above. Amide II modes in the B structures are more tightly clustered than for the A series resulting in more intensity for the overlapped cluster. This is particularly evident in the in vacuom representation, where amide II modes are often predicted to have anomalously high intensity without solvent correction.[21] To lower frequency is a distinct intense F1-p2 C—N stretch, predicted at ~1420 cm^{-1}.

This shift to a representation of the B conformers, in contrast to Figures 9 and 10, was chosen to show the differences in spectra for the two forms which is especially evident in the VCD. Here the dominant pattern seen is a positive amide I couplet, with negative VCD for the lower intensity, higher frequency p2 mode and positive for the intense G3 mode. The other modes also contribute, and with increased mixing tend to have opposing signs, resulting in added couplet (or oscillating) bands, but maintaining a positive couplet overall pattern. The Ala representation for the B-1 conformer in fact results in an alternating sign pattern for the amide I modes (Fig. 11d′) that is in qualitative agreement with the experimental pattern seen in D_2O. This underlying oscillation has a tendency to result in two high frequency negative components being apparent in the VCD, much as seen in TFE experimentally, when the computed dispersion is contracted in the COSMO version for the full peptide. Another facet of this B-series conformation is that the Asp—COOH mode is less separated from the amide I than for the A series, but this characteristic is quite dependent on method. Clustering of the amide II modes seems to result in a negative couplet pattern with the lower frequency negative component being dominant, and quite intense, which does not fit the experimental pattern. The amide II mode is likely to be affected by H-bonding to the solvent, which will vary considerably for different residues. The F1-p2 C—N stretch is also predicted to be negative in this conformation.

DISCUSSION

This study of a model cyclic peptide demonstrates the chirality that develops for a sequence with an averaged set of constrained conformations, as measured with VCD. The VCD spectra of amide I bands have no local character and result from the coupling of locally achiral groups in a chiral conformation. The constraint persists through conformational averaging due to the relative weighting of favored structures. Thus the important issue for interpretation of spectra in terms of conformation is proper modeling of this coupling. Here we showed that the peptide can be adequately represented by its backbone if one keeps in mind the necessary corrections that will be imposed by the side chains, such as spectral overlap and shifting of the base frequencies. This is most easily done if Gly and Pro residues, which are the most distinct vibrational variants, are kept as explicit components of the structure and if other residues are represented as L-Ala, with the proper chirality.

There are certainly solvent effects on the spectra, as can be seen by comparing our IR and VCD data for the cyclic peptide in TFE and water (even more so in DMSO, data not shown). However, the results are qualitatively consistent. This fits the MD results which show that the amide backbone does not change much unless one uses a very high temperature trajectory. The qualitative sign pattern of the VCD transitions is preserved in both spectra. The computed patterns for the B-series in vacuom and with COSMO mostly reflect the observed amide I spectra and actually are somewhat better predicted with the COSMO on the full c(FpGRGD) peptide than the minimal (Ala-based) side-chain simulation. But the qualitative agreement for the amide I is apparent in both levels of computation, while that for the amide II is not. The qualitative success of the Ala prediction arises because the side chains do not contribute much to the amide I VCD pattern, but they do shift the frequencies, much as solvation does, and in this case they distort the low frequency side (due to Arg mode overlap). Use of VCD predicted for just a single structure means that this shift arises from a perturbation due to a fixed, arbitrary stereochemical relationship, whereas the sidechains in solution are highly flexible. Substituting Ala in the prediction means such effects, while ignored, are also effectively averaged. None-the-less the frequency impact remains and one must be aware of it to compensate in the analysis. As we have established, solvation effects can be compensated in VCD analyses by knowing the general effects and either shifting the mode frequencies or just compensating for them in analysis of the

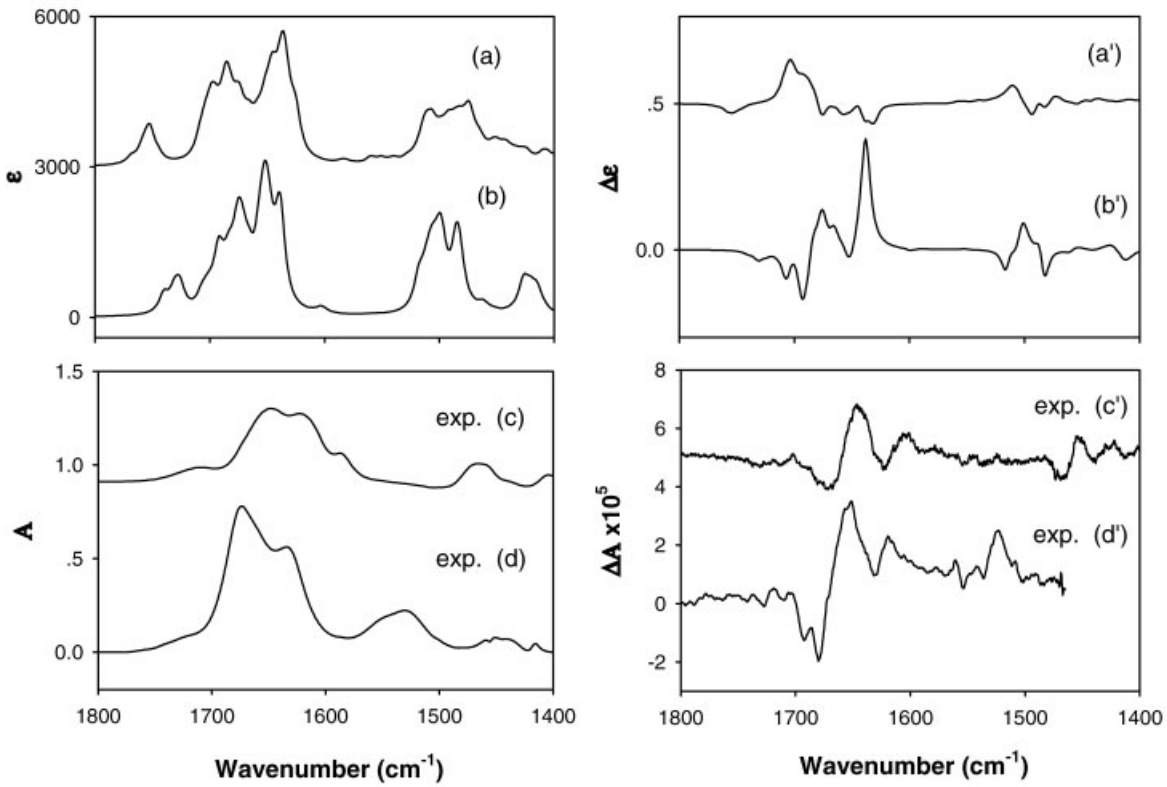

Fig. 12. Comparison of the average IR (left) and VCD (right) spectra for the (**a**) A1-10 Type I′ series and (**b**) B1-4 Type II′ series of computed spectra with the respective experimental spectra in (**c**) D_2O and (**d**) TFE OH.

spectra. The same should be true of flexible side-chain effects. If those effects are tracked by simulation resulting in establishment of behavior patterns, the simpler calculations can lead one to a useful conformational interpretation. The Arg effect is also minimized by N—D substitution which shifts those modes down in wavenumber and reduces overlap with the amide I modes.

Comparison with Experiment

All the spectra we calculated have a dispersed amide I mode typically exhibiting two main overlapped features whose components to lower energy are generally more intense, which reflects the ATR spectral patterns (see Fig. 4) but does not fit the solution results (Fig. 3) as well. The computed spectra of both the A and B series have this pattern, but computationally the A pattern is more dependent on Arg modes being mixed with the amide I. In the A series case, the overall pattern could be seen as two overlapped bands. For the c(FpGRGD) peptide in vacuum or when deuterated, as well as for the Ala version, the original pattern persists despite the increased dispersion and the shift of the Arg modes.

In the experimental spectra, the amide II modes are weak and broad at best, which is consistent with the A-series IR absorbance but not predicted by the B-series pattern. Even with COSMO the amide I–II separation is too large. In our experience, only use of explicit solvent representation in the DFT and a larger basis set including diffuse functions (as suggested above with our Gly_6 comparative calculations in Fig. 9) can overcome this deficiency.[21,66,79] Lower frequency bands do not discriminate between the two structural models, due to low IR intensity; consequently, the IR is seen to be conformationally indeterminant. There are variations in the different conformations found in the MD trajectory, so choosing just one (as done in the above examples using just B-1 or A-4 conformers) biases the result. Averaging over the trajectory should help even out the specific deviations, but this requires computing spectra for individual structural variants. A comparison of the experimental data and the computed average for the selected A and B-forms noted in Table 3 are shown in Figure 12.

VCD does show a distinct difference between the conformers. The B-series has a dominant amide I positive couplet, although when these four spectra are averaged, an anomalously high intensity positive VCD band appears on the low frequency side of the amide I mode. The match of specific modes is far from perfect, and the lower frequency components of the amide I are underrepresented, but the overall sign pattern seen experimentally suggests that the B-conformers must make a major contribution to the conformational mix, and this would in turn indicate that Type

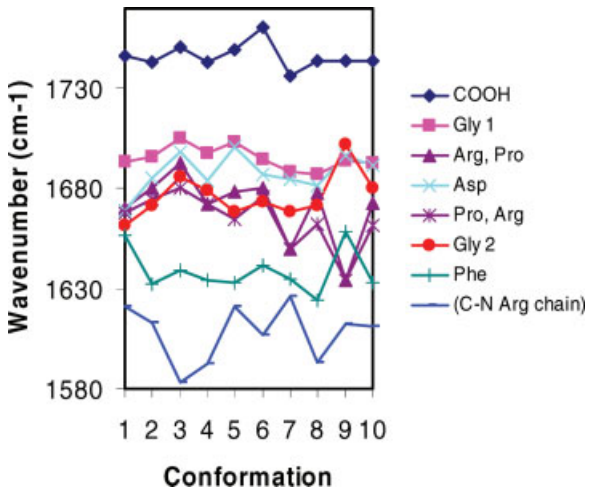

Fig. 13. Calculated amide C=O (and Arg side chain) stretching mode frequencies for 10 A-type conformations of the cyclic peptide selected during the MD run. [Color figure can be viewed in the online issue, which is available at www.interscience.wiley.com.]

II′ turns are important in this cyclic peptide structure. The apparent mis-match in the amide II region noted above for the B-1 conformer is improved by averaging over the four B conformers, making that mode also supportive of this structural assignment. Clearly the only way to find agreement between experiment and theory here is to average computed spectra for many structures. Since our selection of them from the MD trajectory is intrinsically arbitrary, definitive structural analysis is premature, but qualitative conformational determination seems possible. Slight variation (full minimization) of the modeling of the A structures revealed that the VCD pattern is very sensitive to minor geometry variations within one class of the β-turns. Particularly, the increased flexibility of the peptide chain in the vicinity of the glycine residues, observed also for other model oligopeptides,[26] can have a significant impact on the resultant spectral shape.

Going beyond the amide modes, the Asp—COOH mode is experimentally seen as a shoulder on the high frequency side of the amide I, more like the B-series predictions, and the Arg bands are low frequency shoulders (in D_2O, but perhaps higher in organic solvents). Without the COSMO correction, the predicted Asp band would be even more unrealistically high in frequency. The VCD corresponding to this band is very weak and functionally indeterminate in sign. The Arg modes are more difficult to sort out, but apparently are just below the amide I in D_2O and have little VCD contribution. The sum of these observations is that the Ala model offers a representation better suited to assigning the amide modes than do the full side-chain calculations, but that the COSMO corrections remain helpful. This assumption must be used with care. Clearly for peptides containing Arg, there is an upward shift of the F1-p2 frequency, so the Arg has an impact on the amide I, serving to reduce its dispersion. Further, for sorting out these modes, it is very useful to have calculated the spectra at different levels of approximation. By this we mean with varying contributions from the side chains. For a single DFT calculation, the side chain contributions could be shifted by isotopic substitution, which while somewhat difficult (or at least expensive) to realize experimentally, is straightforward to simulate computationally by just changing the masses and reusing the original FF.

We have further attempted to use the empirical corrections for solvent effects that we have previously reported to further correct the spectra for solvent effects (not shown).[81,84,85] Unfortunately, although the corrections did improve the frequencies of the amide I modes, they did not lead to an improved interpretation of the data.

Effect of Molecular Flexibility

Finally, we explore the effect of the conformational flexibility of the peptide on the spectra. This effect, perhaps surprisingly, appears smaller than that of the solvent, at least in the adopted models. For example, for the 10 A-conformations selected during the MD run, amide I frequencies oscillate ($\sim\pm 15\ cm^{-1}$) around average values and the arginine side chain vibration exhibits slightly bigger sensitivity to the conformations. This of course is consistent with the small changes in backbone geometry (see ϕ, ψ values in Table 2), whose impact on amide I frequencies can be seen in Figure 13. There similar normal modes are tracked in different conformers with the aid of the S-vector overlaps, $P_{A_I B_J} = |\sum_{\lambda=1\ldots NAT,\ \alpha=1,3} S^{I,A}_{\lambda\alpha} S^{J,B}_{\lambda\alpha}|$, where $S^{I,A}_{\lambda\alpha}$, is the S-matrix vector for mode I, atom λ and coordinate α in conformation A.[66] The overlaps achieve maximum values (= 1) for identical modes. Occasional change of the transition ordering suggests that the averaging could change the signs of VCD features, which does occur for close lying modes as can be seen in the variations of central frequencies for the 10 conformers, and even sometimes for further separated ones, see conformers A-7 and A-9 as shown in Figure 13. Similar plots could be made for the B-conformers, but they are much more similar and consequently do not offer such exchanges in ordering.

ACKNOWLEDGMENT

We wish to thank Ms. Martha Juban in the LSU Protein Facility for assistance with the peptide synthesis.

LITERATURE CITED

1. Aamouche A, Devlin FJ, Stephens PJ. Determination of the absolute configuration of 1-(2-methylnaphtyl)methyl sulfoxide by vibrational circular dichroism spectroscopy. J Org Chem 2001;66:3671–3677.
2. Beenken WJD, Lischka H. Spectral broadening and diffusion by torsional motion in biphenyl. J Chem Phys 2005;123:144311.
3. Williams RW, Dunker AK. Determination of the secondary structure of proteins from the amide I band of the laser raman spectrum. J Mol Biol 1981;152:783–813.
4. Keiderling TA. Protein and peptide secondary structure and conformational determination with vibrational circular dichroism. Curr Opin Chem Biol 2002;6:682–688.
5. Keiderling TA. Peptide and protein conformational studies with vibrational circular dichroism and related spectroscopies. In: Berova N, Nakanishi K, Woody RW, editors. Circular dichroism: principles and applications, 2nd ed. New York: Wiley-VCH; 2000. p 621–666.

6. Barron LD, Zhu F, Hecht L. Raman optical activity: an incisive probe of chirality and of biomolecular structure and behaviour. Vib Spectrosc 2006;42:15–24.
7. Decatur SM, Antonic J. Isotope-edited FTIR spectroscopy of helical peptides. J Am Chem Soc 1999;121:11914–11915.
8. Barber-Armstrong W, Donaldson T, Wijesooriya H, Silva RAGD, Decatur SM. Empirical relationships between isotope-edited IR spectra and helix geometry in model peptides. J Am Chem Soc 2004;126:2339–2345.
9. Huang R, Kubelka J, Barber-Armstrong W, Silva RAGD, Decatur SM, Keiderling TA. Nature of vibrational coupling in helical peptides: an isotopic labeling study. J Am Chem Soc 2004;126:2346–2354.
10. Silva RAGD, Barber-Armstrong W, Decatur SM. The organization and assembly of a beta-sheet formed by a prion peptide in solution: an isotope-edited FTIR study. J Am Chem Soc 2003;125:13674–13675.
11. Silva RAGD, Nguyen JY, Decatur SM. Probing the effect of side chains on the conformaiton and stability of helical peptides via isotope-edited infrared spectroscopy. Biochemistry 2002;51:15296–15303.
12. Kubelka J, Silva RAGD, Bouř P, Decatur SM, Keiderling TA. Chirality in peptide vibrations. Ab Initio computational studies of length, solvation, hydrogen bond, dipole coupling and isotope effects on vibrational CD. In: Hicks JM, editor. Chirality: physical chemistry. ACS Symposium Series. Vol. 810. Washington DC: American Chemical Society; 2002. p 50–64.
13. Kubelka J, Keiderling TA. The anomalous infrared amide I intensity distribution in ^{13}C isotopically labeled peptide β-sheets comes from extended, multiple-stranded structurres. An ab initio study. J Am Chem Soc 2001;123:6142–6150.
14. Silva RAGD, Kubelka J, Decatur SM, Bouř P, Keiderling TA. Site-specific conformational determination in thermal unfolding studies of helical peptides using vibrational circular dichroism with isotopic substitution. Proc Natl Acad Sci USA 2000;97:8318–8323.
15. Decatur SM. IR spectroscopy of isotope-labeled helical peptides: probing the effect of *N*-acetylation on helix stability. Biopolymers 2000;54:180–185.
16. Starzyk A, Barber-Armstrong W, Sridharan M, Decatur SM. Spectroscopic evidence for backbone desolvation of helical peptides by 2,2,2-trifluoroethanol: an isotope edited IR study. Biochemistry 2005;44:369–376.
17. Bouř P, Keiderling TA. Ab initio modeling of amide I coupling in antiparallel beta-sheets and the effect of 13C isotopic labeling on infrared spectra. J Phys Chem B 2005;109:5348–5357.
18. Decatur SM. Elucidation of residue-level structure and dynamics of polypeptides via isotope-edited infrared spectroscopy. Acc Chem Res 2006;39:169–175.
19. Sreerama N, Woody RW. Protein secondary structure from circular dichroism spectroscopy—combining variable selection principle and cluster analyses with neural network, ridge regression and self-consistent methods. J Mol Biol 1994;242:497–507.
20. Venyaminov SY, Yang JT. Determination of protein secondary structure. In: Fasman GD, editor. Circular dichroism and the conformational analysis of biomolecules. New York: Plenum; 1996. p 69–107.
21. Kubelka J, Huang R, Keiderling TA. Solvent effects on IR and VCD spectra of helical peptides: DFT-based static spectral simulations with explicit water. J Phys Chem B 2005;109:8231–8243.
22. Hollosi M, Majer ZS, Ronai AZ, Magyar A, Medzihradszy K, Holly S, Perczel A, Fasman GD. CD and Fourier transform IR spectroscopic studies of peptides. II. Detection of beta turns in linear peptides. Biopolymers 1994;34:177–185.
23. Vass E, Kurz M, Konat RK, Hollosi M. FTIR and CD spectroscopic studies on cyclic penta- and hexa-peptides. Detailed examination of hydrogen bonding in (beta)- and (gamma)- turns determined by NMR. Spectrochim Acta 1998;54:773–786.
24. Perczel A, Hollosi M. Turns. In: Fasman GD, editor. Circular dichroism and the conformational analysis of biomolecules. New York: Plenum; 1996. p 285.
25. Vass E, Hollosi M, Besson F, Buchet R. Vibrational spectroscopic detection of beta- and gamma-turns in synthetic and natural peptides and proteins. Chem Rev 2003;103:1917–1954.
26. Kim J, Kapitán J, Lakhani A, Bouř P, Keiderling TA. Tight β-turns in peptides. DFT-based study of infrared absorption and vibrational circular dichroism for various conformers including solvent effects. Theor Chem Acc 2008;119:81–97.
27. Krishnan B, Szymanska A, Gierasch LM. Site-specific fluorescent labeling of poly-histidine sequences using a metal-chelating cysteine. Chem Biol Drug Des 2007;69:31–40.
28. Roy RS, Gopi HN, Raghothama S, Karle IL, Balaram P. Hybrid peptide hairpins containing alpha- and omega-amino acids: conformational analysis of decapeptides with unsubstituted beta-, gamma-, and delta-residues at positions 3 and 8. Chem A Eur J 2006;12:3295–3302.
29. Mahalakshmi R, Raghothama S, Balaram P. NMR analysis of aromatic interactions in designed peptide beta-hairpins. J Am Chem Soc 2006;128:1125–1138.
30. Syud FA, Stanger HE, Mortell HS, Espinosa JF, Fisk JD, Fry CG, Gellman SH. Influence of strand number on antiparallel beta-sheet stability in designed three- and four-stranded beta-sheets. J Mol Biol 2003;326:553–568.
31. Karle I, Gopi HN, Balaram P. Infinite pleated beta-sheet formed by the beta-hairpin Boc-beta-Phe-beta-Phe-D-Pro-Gly-beta-Phe-beta-Phe-OMe. Proc Natl Acad Sci USA 2002;99:5160–5164.
32. Setnička V, Huang R, Thomas CL, Etienne MA, Kubelka J, Hammer RP, Keiderling TA. IR study of cross-strand coupling in a beta-hairpin peptide using isotopic labels. J Am Chem Soc 2005;127:4992–4993.
33. Ramirez-Alvarado M, Kortemme T, Blanco FJ, Serrano L. Beta-hairpin and beta-sheet formation in designed linear peptides. Bioorg Med Chem 1999;7:93–103.
34. Lacroix E, Kortemme T, Lopez de la Paz M, Serrano L. The design of linear peptides that fold as monomeric β-sheet structures. Curr Opin Struct Biol 1999;9:487–493.
35. Kortemme T, Ramirez-Alvarado M, Serrano L. Design of a 20-amino acid, three-stranded beta-sheet protein. Science 1998;281:253–256.
36. Hilario J, Kubelka J, Syud FA, Gellman SH, Keiderling TA. Spectroscopic characterization of selected β-sheet hairpin models. Biospectroscopy 2002;67:233–236.
37. Espinosa JF, Syud FA, Gellman SH. Analysis of the factors that stabilize a designed two-stranded antiparallel beta-sheet. Protein Sci 2002;11:1492–1505.
38. Hilario J, Kubelka J, Keiderling TA. Optical spectroscopic investigations of model beta-sheet hairpins in aqueous solution. J Am Chem Soc 2003;125:7562–7574.
39. Koepf EK, Petrassi HM, Sudol M, Kelly JW. WW: an isolated three-stranded antiparallel beta-sheet domain that unfolds and refolds reversibly; evidence for a structured hydrophobic cluster in urea and GdnHCl and a disordered thermal unfolded state. Protein Sci 1999;8: 841–853.
40. Bouř P, Keiderling TA. Vibrational spectral simulation for peptides of mixed secondary structure: method comparisons with the Trpzip model hairpin. J Phys Chem B 2005;109:23687–23697.
41. Bouř P, Buděšínský M, Špirko V, Kapitán J, Šebestík J, Sychrovský V. A complete set of NMR chemical shifts and spin-spin coupling constants for L-alanyl-L-alanine zwitterion and analysis of its conformational behavior. J Am Chem Soc 2005;127:17079–17089.
42. Yasui SC, Pančoška P, Dukor RK, Keiderling TA, Renugopalakrishnan V, Glimcher MJ, Clark RC. Conformational transitions of phosvitin with pH variation. Vibrational circular dichroism study. J Biol Chem 1990;265:3780–3788.
43. Mantsch HH, Perczel A, Hollosi M, Fasman GD. Characterization of β-turns in cyclic hexapeptides in solution by Fourier transform IR spectroscopy. Biopolymers 1993;33:201–207.
44. Vass E, Lang E, Samu J, Majer Z, Kajtar-Peredy M, Mak M, Radics I, Hollosi M. Vibrational spectrocopic detection of H-bonded β- and γ-turns in cyclic peptides and glycopeptides. J Mol Struct 1998;440:59–71.
45. Cochran AG, Tong RT, Starovasnik MA, Park EJ, McDowell RS, Theaker JE, Skelton NJ. Minimal peptides scaffold for beta-turn display: optimizing a strand position in disulfide-cyclized beta-hairpins. J Am Chem Soc 2001;123:625–632.
46. Ravi A, Balaram P. Cyclic peptide disulfides. Consecutive beta-turn conformation of a synthetic model peptide corresponding to the active site of thioredoxin. Biochi Biophys Acta 1983;745:301–309.

47. García-Echeverría C, Siligardi G, Mascagni P, Gibbons W, Giralt E, Pons M. Conformational analysis of two cyclic disulfide peptides. Biopolymers 1991;31:835–843.
48. Russell SJ, Blandl T, Skelton NJ, Cochran AG. Stability of cyclic beta-hairpins: asymmetric contributions from side chains of a hydrogen-bonded cross-strand residue pair. J Am Chem Soc 2003;125:388–395.
49. Ravi A, Prasad BVV, Balaram P. Cyclic peptide disulfides—solution and solid-state conformation of Boc-Cys-Pro-Aib-Cys-S-S-bridge-NH-Me, a disulfide-bridged peptide helix. J Am Chem Soc 1983;105:105–109.
50. Xie P, Zhou QW, Diem M. Conformational studies of β-turns in cyclic peptides by vibrational CD. J Am Chem Soc 1995;117:9502–9508.
51. Gilon C, Mang C, Lohof E, Friedler A, Kessler H. In: Goodman M, Felix A, Moroder L, Toniolo C, editors. Synthesis of peptides and peptidomimetics, Vol. E 22 b. New York: Georg Thieme Verlag Stuttgart; 2003. p 461.
52. Perczel A, Hollosi M, Foxman BM, Fasman GD. Conformational analysis of pseudocyclic hexapeptides based on quantitative circular dichroism (CD), NOE, and X-ray data. The pure CD spectra of Type I and Type II beta-turns. J Am Chem Soc 1991;113:9772–9784.
53. Matter H, Kessler H. Structures, dynamics, and biological activities of 15 cyclic hexapeptide analogs of the alpha-amylase inhibitor tendamistat (HOE 467) in solution. J Am Chem Soc 1995;117:3347–3359.
54. Gardner RR, Liang GB, Gellman SH. Beta-turn and beta-hairpin mimicry with tetrasubstituted alkenes. J Am Chem Soc 1999;121:1806–1816.
55. Kaul R, Angeles AR, Jager M, Powers ET, Kelly JW. Incorporating beta-turns and a turn mimetic out of context in loop 1 of the WW domain affords cooperatively folded beta-sheets. J Am Chem Soc 2001;123:5206–5212.
56. Syud FA, Stanger HE, Gellman SH. Interstrand side chain-side chain interactions in a designed β-hairpin: significance of both lateral and diagonal pairings. J Am Chem Soc 2001;123:8667–8677.
57. Cochran AG, Skelton NJ, Starovasnik MA. Tryptophan zippers: stable, monomeric beta-hairpins. Proc Natl Acad Sci USA 2001;98:5578–5583.
58. Chatterjee J, Mierke D, Kessler H. *N*-methylated cyclic pentaalanine peptides as template structures. J Am Chem Soc 2006;128:15164–15172.
59. Kessler H, Bats JW, Griesinger C, Koll S, Will M, Wagner K. Peptide conformations. 46. Conformational analysis of a superpotent cytoprotective cyclic somatostatin analog. J Am Chem Soc 1988;110:1033–1049.
60. Gierasch LM, Deber CM, Madison V, Niu CH, Blout ER. Conformations of (X-L-Pro-Y)2 cyclic hexapeptides. Preferred beta-turn conformers and implications for beta turns in proteins. Biochemistry 1981;20:4730–4738.
61. Bean JW, Kopple KD, Peishoff CE. Conformational analysis of cyclic hexapeptides containing the D-Pro-L-Pro sequence to fix beta-turn positions. J Am Chem Soc 1992;114:5328–5334.
62. Muller G, Gurrath M, Kurz M, Kessler H. BetaVI turns in peptides and proteins: a model peptide mimicry. Protein Struct 1993;15:235–251.
63. Kubelka J, Keiderling TA. Differentiation of β-sheet forming structures: ab initio based simulations of IR absorption and vibrational CD for model peptide and protein β-sheets. J Am Chem Soc 2001;123:12048–12058.
64. Huang R, Setnička V, Etienne MA, Kim J, Kubelka J, Hammer RP, Keiderling TA. Cross-strand coupling of a β-hairpin peptide stabilized with an Aib-Gly turn using isotope-edited IR spectroscopy. J Am Chem Soc 2007;129:13592–13603.
65. Bouř P, Sopková J, Bednárová L, Maloň P, Keiderling TA. Transfer of molecular property tensors in Cartesian coordinates: a new algorithm for simulation of vibrational spectra. J Comput Chem 1997;18:646–659.
66. Kim J, Huang R, Kubelka J, Bouř P, Keiderling TA. Simulation of infrared spectra for beta-hairpin peptides stabilized by an Aib-Gly turn sequence: correlation between conformational fluctuation and vibrational coupling. J Phys Chem B 2006;110:23590–23602.
67. Kapitán J, Baumruk V, Kopecký VJ, Bouř P. Demonstration of the ring conformation in polyproline by the Raman optical activity. J Am Chem Soc 2006;128:2438–2443.
68. Bouř P. Computations of the Raman optical activity via the sum-over-states expansions. J Comput Chem 2001;22:426–435.
69. Barany G, Albericio F. A 3-dimensional orthogonal protection scheme for solid-phase peptide-synthesis under mild conditions. J Am Chem Soc 1985;107:4936–4942.
70. Kates SA, Sole NA, Johnson CR, Hudson D, Barany G, Albericio F. A novel, convenient, 3-dimensional orthogonal strategy for solid-phase synthesis of cyclic-peptides. Tetrahedron Lett 1993;34:1549–1552.
71. Albericio F, Cases M, Alsina J, Triolo SA, Carpino LA, Kates SA. On the use of PyAOP, a phosphonium salt derived from HOAt, in solid-phase peptide synthesis. Tetrahedron Lett 1997;38:4853–4856.
72. Keiderling TA, Kubelka J, Hilario J. Vibrational circular dichroism of biopolymers. Summary of methods and applications. In: Braiman M, Gregoriou V, editors. Vibrational spectroscopy of polymers and biological systems. Boca Raton: CRC Press; 2006. p 253–324.
73. Ponder JW. Tinker, software tools for molecular design v. 4.2. 2004; Available at: http://dasher.wustl.edu/tinker/.
74. Pearlman DA, Case DA, Caldwell JW, Ross WS, Cheatham TE, Debolt S, Ferguson DM, Seibel G, Kollman PA. AMBER, a package of computer progeams for applying molecular mechanics, normal mode analysis, molecular dynamics and free energy calculations to simulate the structural and energetic properties of molecules. Comp Phys Commun 1995;91:1–41.
75. Jorgensen WL, Chandrasekhar J, Madura JD. Comparison of simple potential fuctions for simulating liquid water. J Chem Phys 1983;79:926–935.
76. Frisch MJ, Trucks GW, Schlegel HB, Scuseria GE, Robb MA, Cheeseman JR, Montgomery JA, Vreven T, Kudin KN, Burant JC, Dapprich S, Millam JM, Daniels AD, Kudin KN, Strain MC, Farkas O, Tomasi J, Barone V, Cossi M, Cammi R, Mennucci B, Pomelli C, Adamo C, Clifford S, Ochterski J, Petersson GA, Ayala PY, Cui Q, Morokuma K, Salvador P, Dannenberg JJ, Malick DK, Rabuck AD, Raghavachari K, Foresman JB, Cioslowski J, Ortiz JV, Baboul AG, Stefanov BB, Liu G, Liashenko A, Piskorz P, Komaromi I, Gomperts R, Martin RL, Fox DJ, Keith T, Al-Laham MA, Peng CY, Nanayakkara A, Challacombe M, Gill PMW, Johnson B, Chen W, Wong MW, Andres JL, Gonzalez C, Head-Gordon M, Replogie ES, Pople. Gaussian 03, Revision C .02. Wallingford CT: Gaussian, Inc.; 2004.
77. Bouř P, Keiderling TA. Partial optimization of molecular geometry in normal coordinates and use as a tool for simulation of vibrational spectra. J Chem Phys 2002;117:4126–4132.
78. Bouř P. Convergence properties of the normal mode optimization and its combination with molecular geometry constraints. Collect Czech Chem Commun 2005;70:1315–1340.
79. Kubelka J, Keiderling TA. Ab initio calculation of amide carbonyl stretch vibrational frequencies in solution with modified basis sets. 1. *N*-methyl acetamide. J Phys Chem A 2001;105:10922–10928.
80. Bouř P, Michalík D, Kapitán J. Empirical solvent correction for multiple amide group vibrational modes. J Chem Phys 2005;122:144501.
81. Bouř P. On the influence of the water electrostatic field on the amide group vibrational frequencies. J Chem Phys 2004;121:7545–7548.
82. Kubelka J, Silva RAGD, Keiderling TA. Discrimination between peptide 3_{10}- and α-helices. Theoretical analysis of the impact of α-methyl substitution on experimental spectra. J Am Chem Soc 2002;124:5325–5332.
83. Bouř P, Kubelka J, Keiderling TA. Quantum mechanical models of peptide helices and their vibrational spectra. Biopolymers 2002;65:45–69.
84. Bouř P, Keiderling TA. Empirical modeling of the peptide amide I band IR intensity in water solution. J Chem Phys 2003;119:11253–11262.
85. Yang S, Cho M. IR spectra of *N*-methylacetamide in water predicted by combined quantum mechanical/molecular mechanical molecular dynamics simulations. J Chem Phys 2005;123:134503.